Obtaining Absorptive Line Shapes in Two-Dimensional Infrared Vibrational Correlation Spectra

M. Khalil, N. Demirdöven, and A. Tokmakoff

Department of Chemistry, Massachusetts Institute of Technology, Cambridge, Massachusetts 02139

(Received 12 April 2002; published 30 January 2003)

Absorptive line shapes in two-dimensional infrared (2D IR) vibrational spectra are important for an intuitive interpretation of molecular structure and dynamics. We obtain an absorptive 2D IR correlation spectrum by summing complementary spectra from experiments sampling vibrational coherences that oscillate with conjugate frequencies in the initial evolution time period. The 2D correlation spectrum of a coupled vibrational system reveals certain spectral features with tilted line shapes that are explained in terms of unequal contributions of Liouville-space pathways.

DOI: 10.1103/PhysRevLett.90.047401 PACS numbers: 78.30.–j, 39.30.+w, 42.50.Md, 78.47.+p

Understanding molecular interactions in the condensed phase requires experimental tools that can simultaneously follow the time evolution of multiple coordinates. Borrowing ideas from multidimensional nuclear magnetic resonance (NMR), two-dimensional infrared (2D IR) spectroscopy has been developed to address these issues. It has been successful in measuring vibrational couplings, discriminating between different line-broadening mechanisms, and capturing transient structure on a picosecond time scale [1–6]. 2D IR spectroscopy is a pulsed Fourier transform technique where sequences of femtosecond (fs) IR fields with varying delays manipulate coherences in a system of coupled vibrations. The resultant data is Fourier transformed and represented as a 2D correlation map of frequencies sampled during the initial evolution and final detection time periods. Molecular information is encoded in the positions, amplitudes and line shapes of the various resonances in a 2D vibrational spectrum. Inversion of the experimental spectrum to gain insight into the properties of the material Hamiltonian becomes nontrivial for congested 2D spectra with overlapping resonances. It requires optimizing experimental methods to collect intuitive 2D spectra and developing theoretical tools to simulate them. Obtaining absorptive line shapes is the first step in measuring an intuitive 2D vibrational spectrum where the signs and positions of close-lying resonances are well resolved.

NMR spectroscopy uses phase cycling methods to obtain 2D spin correlation spectra with absorptive peaks. This involves selecting signals where spins precess in opposite directions during the evolution period [7]. The generation and manipulation of fs IR pulses and the samples they investigate differs greatly from the well-established NMR techniques and in general there does not exist a one-to-one correspondence between the two experimental methodologies. In nonlinear optical and IR spectroscopy, detecting the signal in a phase-matched direction and varying the sequence of input pulses substitutes for much of the phase cycling used to obtain absorptive line shapes in NMR spectra [8–12]. Following this idea, we perform two different IR experiments sampling conjugate frequencies during the initial time period. The sum of the heterodyne-detected 2D spectra resulting from these two experiments gives a 2D IR vibrational correlation spectrum with absorptive line shapes. 2D electronic correlation spectroscopy sampling conjugate frequencies in the evolution period have been performed using noncollinear pulses and phase-locked pump-probe techniques [11,13].

In this Letter, we report on obtaining a 2D IR vibrational correlation spectrum with absorptive features of the anharmonic carbonyl stretches of dicarbonylacetylacetonato rhodium (I) (RDC) dissolved in hexane. The 2D IR spectroscopy of this model system is described in terms of six vibrational states: 0, a, s, $2a$, as, and $2s$; where a and s represent one quantum of energy in the asymmetric and symmetric C≡O stretches, respectively [5,14]. Because of the presence of the overtones ($2a$, $2s$) and the combination band (as), the 2D IR vibrational correlation spectrum is sensitive to Liouville-space pathways involving four different dipole interactions, which results in certain peaks having partially phase-twisted character. The transitions between the one and two-quantum states in a coupled vibrational system make the reported 2D correlation spectrum distinct from 2D spectra of electronic states and coupled nuclear spins.

The 2D IR experiment is a heterodyne-detected, resonant third-order nonlinear technique where three mid-IR fs input fields $\boldsymbol{E}_a$,$\boldsymbol{E}_b$, and $\boldsymbol{E}_c$, each with a unique incident wave vector $\boldsymbol{k}_a$,$\boldsymbol{k}_b$, and $\boldsymbol{k}_c$, cross in the sample to radiate a signal field into the $\boldsymbol{k}_s = -\boldsymbol{k}_a + \boldsymbol{k}_b + \boldsymbol{k}_c$ phase-matched direction. The vibrational transition frequencies between the six vibrational states are probed during three independent time periods referred to as the evolution (τ_1), waiting (τ_2), and detection (τ_3) periods corresponding to the delay between the three input pulses as shown in Fig. 1. By selecting particular time orderings (1, 2, 3) for the incident wave vectors (a, b, c), three possible experiments can be constructed that observe signal along $\boldsymbol{k}_s$: $S_{\mathrm{I}} = -\boldsymbol{k}_1 + \boldsymbol{k}_2 + \boldsymbol{k}_3$, $S_{\mathrm{II}} = +\boldsymbol{k}_1 - \boldsymbol{k}_2 + \boldsymbol{k}_3$, and

 0031-9007/03/90(4)/047401(4)$20.00

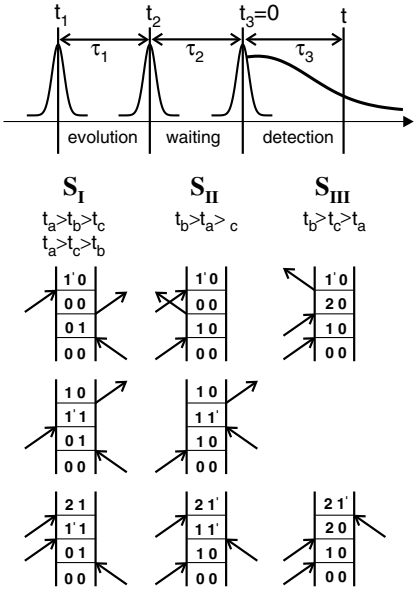

FIG. 1. The pulse sequence and Liouville interaction pathways for third-order nonlinear 2D IR spectroscopy. The variables t_n and τ_n represent the center of the three input pulses and the delays between them to generate a third-order nonlinear polarization at time t. The double-sided Feynman diagrams contributing to the rephasing and nonrephasing Liouville-space pathways for particular pulse orderings. The numbering 0, 1 and $1'$ and 2 represent the ground, first and second excited states of a multilevel vibrational system. For this particular system, $1, 1' \in \{a, s\}$ and $2 \in \{2a, as, 2s\}$.

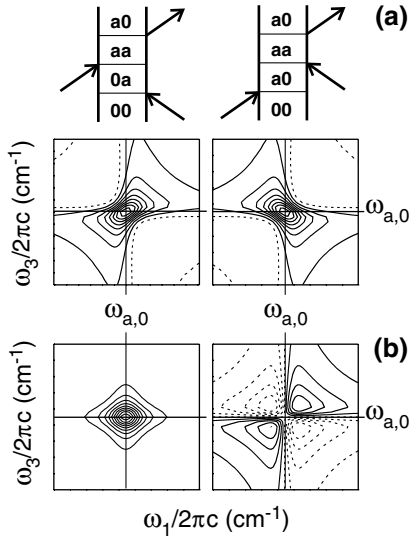

FIG. 2. (a) The Feynman diagrams for a particular rephasing and nonrephasing pathway and the corresponding 2D phase-twisted line shapes. (b) Purely absorptive (left) and dispersive (right) line shapes obtained from the addition and subtraction of the rephasing and nonrephasing signals. Solid and dashed lines indicate the positive and negative contours, respectively.

$S_{\mathrm{III}} = +\boldsymbol{k}_1 + \boldsymbol{k}_2 - \boldsymbol{k}_3$ [10]. These experiments can be broadly classified as rephasing and nonrephasing experiments, which sample Liouville pathways illustrated by the double-sided Feynman diagrams in Fig. 1. The rephasing (or echo) experiment selects S_{I} processes in which the system evolves in conjugate frequencies during τ_1 and τ_3. The nonrephasing (or virtual echo) experiment samples S_{II} and S_{III} pathways with the system evolving with the same vibrational phase during τ_1 and τ_3. Contributions from S_{III} arise only for multilevel systems as illustrated in Fig. 1.

To understand why the addition of equally weighted rephasing and nonrephasing signals results in a purely absorptive line shape, consider the pathways S_R and S_{NR} represented by the two Feynman diagrams shown in Fig. 2(a) and their corresponding 2D line shapes. The response functions for S_R and S_{NR} in the motionally narrowed limit differ only in the phase of the frequency during τ_1 [8]. The line shape observed in a 2D IR measurement is related to the 2D Fourier cosine transform of the data collected as a function of the evolution and detection time periods. The rephasing and nonrephasing 2D spectra show a phase-twisted line shape tilted along the diagonal and the off-diagonal axes, respectively. This phase twist arises because the 2D Fourier cosine transform of a signal evolving with complex phase in two time periods leads to a combination of absorptive and dispersive features [7]. The dispersive wings effectively broaden the linewidth of the transitions and distort their shape, making it difficult to resolve overlapping resonances and interpret the underlying structure. When the rephasing and nonrephasing 2D spectra are added, the dispersive wings cancel to yield a purely absorptive line shape shown in Fig. 2(b). The resultant purely absorptive line shape is dependent on the addition of equally weighted rephasing and nonrephasing pathways.

The 2D IR experiments on RDC in hexane were performed with near-transform limited 90 fs pulses centered at 2050 cm^{-1} (4.9 μm) with a bandwidth of $\sim$160 cm^{-1} [5,15]. The experiment consists of a five-beam interferometer, in which the entering IR pulse train is initially split into four pulses. Three input fields $\boldsymbol{E}_a$, $\boldsymbol{E}_b$, and $\boldsymbol{E}_c$, arranged in a boxcar geometry are focused to a 150 μm diameter in the sample with $\sim$50 nJ of incident energy in each pulse. In the rephasing experiment, $\boldsymbol{E}_a$ precedes $\boldsymbol{E}_b$ and $\boldsymbol{E}_c$, and in the nonrephasing experiment, $\boldsymbol{E}_b$ pre cedes $\boldsymbol{E}_a$ and $\boldsymbol{E}_c$. For each experiment, the second and third pulses are set time-coincident ($\tau_2 = 0$). The remaining fourth beam is split into a local oscillator (LO) and a tracer beam. The tracer beam is sent along the path of the signal and is blocked during collection of the nonlinear signals. Zero timing between the three input beams and the tracer was set to within $\pm$5 fs by taking background-free intensity autocorrelations of each pulse pair in a $AgGaS_2$ crystal placed in the sample plane. After the sample, the emitted signal field is spatially and temporally overlapped with the LO and dispersed in a 190 mm monochrometer with a 150 lines/mm grating.

The dispersed signal is collected at the focal plane with a MCT array detector consisting of 64 pixels, each of which is 100 μm wide. The timing between the LO and the signal was set to within ± 25 fs by measuring their interference with a single channel detector before they entered the monochrometer. The experiments used a 2×10^{-3} M solution of RDC in hexane corresponding to a peak optical density of 0.2 in a 200 μm thick CaF_2 sample cell.

Arrays of dispersed heterodyned signals with a spectral resolution of ~ 1.3 cm^{-1} in the ω_3 dimension were collected as a function of τ_1 for both rephasing and nonrephasing configurations. The τ_1 timing was determined to within ± 1 fs by recombining pulses $\boldsymbol{E}_a$ and $\boldsymbol{E}_b$ after the sample and dispersing them in a second monochrometer. Interference fringes collected at 1975 cm^{-1} as a function of the delay between the two pulses were used to calibrate the τ_1 axis. A Fourier cosine transform along the τ_1 axis yields the individual 2D rephasing and nonrephasing spectra, and the sum of these gives the 2D IR correlation spectrum. The resolution in the ω_1 dimension after Fourier transformation is 1 cm^{-1}. To help in phasing the spectra, a dispersed pump-probe data set using the tracer as the probe and $\boldsymbol{E}_a$ as the pump was taken immediately after collecting the rephasing and nonrephasing scans. The projection of the 2D IR correlation spectrum onto ω_3: $\int S(\omega_1, \omega_3, \tau_2) d\omega_1$ must equal the dispersed pump-probe data taken at the same τ_2. The rephasing and nonrephasing 2D spectra were phased by multiplying the entire dataset by a factor of $\exp[-i\omega_1 \Delta\tau_1 + i\phi]$ to obtain absorptive line shapes for slices taken along the fundamental resonances of $\omega_3 = \omega_{a,0}$ and $\omega_3 = \omega_{s,0}$ and to fit the ω_3 projection of their addition to the dispersed pump-probe dataset.

The rephasing and nonrephasing 2D spectra and their sum are shown in Fig. 3. The first two panels representing the rephasing and nonrephasing pathways show phase-twisted line shapes elongated along the diagonal and the off-diagonal axes. Their sum, plotted on the last panel, is the absorptive 2D IR correlation spectrum, where the dispersive lobes are canceled from the addition of the 2D rephasing and nonrephasing spectra. The 2D IR correlation spectrum shows ten peaks, which arise as a result of the system sampling the Liouville-space pathways shown in Fig. 1. The positions, amplitudes, and line shapes of the resonances are related to the anharmonicity in the nuclear potential, relative orientations, and the system-bath interactions of the coupled carbonyl stretches with the solvent [5]. The positive contributions involve processes in which the system evolves on the fundamental transitions during τ_3, whereas the negative features arise from coherences involving the doubly excited states.

To facilitate a comparison of the rephasing and nonrephasing 2D spectra, the five resonances lying along $\omega_1 = \omega_{a,0}$ have been labeled. We observe that the diagonal peaks (1 and 3) have nearly similar amplitudes, but the cross peak (2 and 4) amplitudes are unequal in the two different measurements. Furthermore, the resonance labeled as 5 is present only in the nonrephasing measurement. A closer look at the Liouville-space pathways in Fig. 1 reveals an inherent imbalance of interaction pathways leading to the formation of the various peaks in the rephasing and nonrephasing spectra for this multilevel system [16]. For example, there are twice the number of diagrams giving rise to peak 2 in the rephasing than in the nonrephasing experiment for any τ_2. Peak 5, which involves four different dipole interactions, is sampled only by the nonrephasing experiment for all τ_2 delays. At $\tau_2 = 0$ contributions from two indistinguishable pulse orderings *a-b-c* and *a-c-b* give rise to the same response function S_{I} in the rephasing signal. The rephasing response functions are complemented by the nonrephasing response functions of S_{II} and S_{III} for indistinguishable pulse orderings *b-a-c* and *b-c-a*, respectively. Simulations of the individual S_{II} and S_{III} response functions reveal that they give rise to the same ten peaks shown in the 2D nonrephasing spectrum in the second panel of Fig. 3. The presence of the S_{III} contribution at $\tau_2 = 0$ in the nonrephasing response for this multilevel system avoids the discontinuity at $\tau_1 = 0$ which has been predicted and observed for a two-level system [17,18].

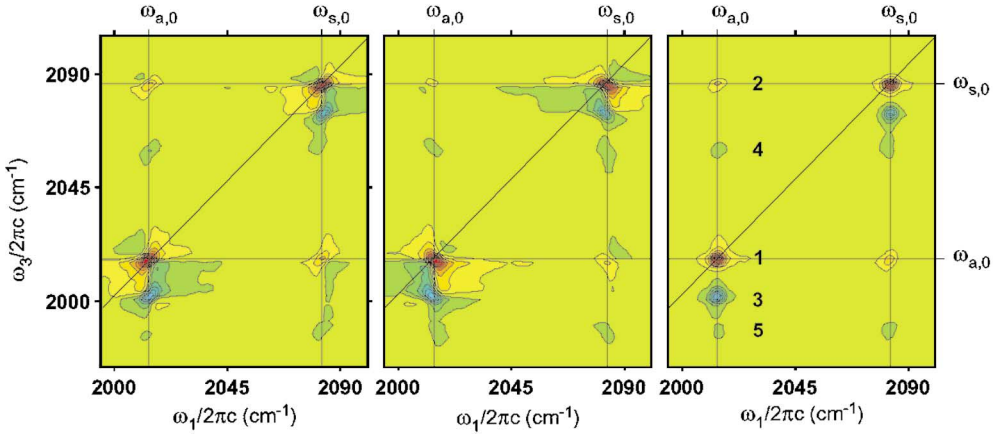

FIG. 3 (color). The 2D IR rephasing spectrum, 2D IR nonrephasing spectrum, and their sum, the 2D IR correlation spectrum, for RDC in hexane. Fifteen equally spaced contour levels from minimum to the maximum value are drawn for each 2D plot.

The imbalance of Liouville-space pathways in the rephasing and nonrephasing experiments leads to line shapes with mixed-phase character in the 2D IR correlation spectrum. In particular, we see that the cross peaks (2 and 4) are tilted by an angle of approximately $\pi/10$ from the ω_1 axis while the diagonal peaks (1 and 3) are nearly symmetric about their resonance frequencies. An angle Ψ can be defined to reflect the degree of phase twist for a 2D line shape through its tilt from the ω_1 axis and it can be related to the relative amplitudes of the rephasing (A_R) and nonrephasing (A_{NR}) spectra by $\tan(\Psi) = (A_R - A_{NR})/(A_R + A_{NR})$ [7]. When $A_{NR} < A_R$ implying that $0 < \Psi < \pi/4$, the 2D line shape is tilted along the diagonal axis. It is tilted in the opposite direction when $A_{NR} > A_R$ and $\pi/2 < \Psi < 3\pi/4$. In light of the above discussion, an angle of $\Psi \approx \pi/10$ for the cross peaks in the last panel of Fig. 3 implies that $A_R = 2A_{NR}$ as is apparent from the 2D rephasing and nonrephasing spectra.

Other than the imbalance of pathways, there are microscopic factors affecting the relative amplitudes of the rephasing and nonrephasing pathways and resulting in the phase-twisted line shapes in the 2D IR correlation spectrum. These include (i) the effect of different dephasing dynamics sampled in rephasing and nonrephasing experiments, (ii) inhomogeneity in the system and the degree of correlation of inhomogeneity between the coupled modes [3,4], (iii) the amplitude of the dipole products for particular peaks in the two different signals, and (iv) the different orientational contributions to the rephasing and nonrephasing spectra depending on which tensor component of the nonlinear signal is measured [19]. 2D electronic correlation spectra indicate that the presence of a Stokes shift would also lead to a phase twist in the 2D electronic correlation spectrum [11,20]. In general, the angle Ψ is also affected by the timing and optical phase of the fs pulses used to excite and detect the third-order nonlinear polarization. The phasing process described earlier corrects for timing errors between the first two pulses. The imbalance of rephasing and nonrephasing pathways is absent in the double resonance, spectrally dispersed pump-probe experiments employing a narrow-band pump-pulse. These experiments do not sample Liouville pathways evolving in a superposition of the fundamental states during the waiting period because the first two interactions originate from the same narrow-band pump-pulse [6].

In conclusion, we have shown that controlling the sequence of the input pulses to obtain 2D IR correlation spectra from rephasing and nonrephasing experiments produces spectra where the position, sign, and shape of the resonances are clear. This method largely eliminates the phase twist that broadens resonances, and reveals the proper sign of peaks that was hidden in previously measured absolute value rephasing spectra. In that respect, this technique holds great promise for simplifying 2D IR spectra of systems with complicated broadening mechanisms and closely lying resonances. In particular, it will help reveal the splitting of cross peaks when the strength of coupling between vibrations is on the order of their vibrational line width. We anticipate that the analysis of independently measured rephasing and nonrephasing 2D IR spectra at varying τ_2 delays and arbitrary polarization of all the input fields will lead to selective ways of enhancing or suppressing features in the 2D IR spectrum.

This work was supported by the U.S. Department of Energy. Additional support was provided by the NSF, ACS-Petroleum Research Fund and the Packard Foundation.

[1] O. Golonzka *et al.*, Phys. Rev. Lett. **86**, 2154 (2001).
[2] M. T. Zanni and R. M. Hochstrasser, Curr. Opin. Struct. Biol. **11**, 516 (2001).
[3] N. Demirdöven, M. Khalil, and A. Tokmakoff, Phys. Rev. Lett. **89**, 237401 (2002).
[4] N.-H. Ge, M. T. Zanni, and R. M. Hochstrasser, J. Phys. Chem. A **106**, 962 (2002).
[5] O. Golonzka *et al.*, J. Chem. Phys. **115**, 10 814 (2001).
[6] S. Woutersen and P. Hamm, J. Phys. Chem. B **104**, 11 316 (2000).
[7] R. R. Ernst, G. Bodenhausen, and A. Wokaun, *Principles of Nuclear Magnetic Resonance in One and Two Dimensions* (Oxford University Press, Oxford, 1987).
[8] S. Mukamel, *Principles of Nonlinear Optical Spectroscopy* (Oxford University Press, New York, 1995).
[9] D. Keusters, H.-S. Tan, and W. S. Warren, J. Phys. Chem. A **103**, 10 369 (1999).
[10] C. Scheurer and S. Mukamel, J. Chem. Phys. **115**, 4989 (2001).
[11] J. D. Hybl, A. A. Ferro, and D. M. Jonas, J. Chem. Phys. **115**, 6606 (2001).
[12] S. M. Gallagher Faeder and D. M. Jonas, J. Phys. Chem. A **103**, 10 489 (1999).
[13] W. P. de Boeij, M. S. Pshenichnikov, and D. A. Wiersma, Annu. Rev. Phys. Chem. **49**, 99 (1998).
[14] J. D. Beckerle *et al.*, Chem. Phys. **160**, 487 (1992).
[15] N. Demirdöven *et al.*, Opt. Lett. **27**, 433 (2002).
[16] See EPAPS Document No. E-PRLTAO-90-032303 for Feynman diagrams that illustrate the imbalance of rephasing and nonrephasing pathways in multilevel vibrational system. A direct link to this document may be found in the online article's HTML reference section. The document may also be reached via the EPAPS homepage (http://www.aip.org/pubservs/epaps.html) or from ftp.aip.org in the directory /epaps/. See the EPAPS homepage for more information.
[17] J. D. Hybl *et al.*, J. Lumin. **87–89**, 126 (2000).
[18] S. M. Gallagher Faeder and D. M. Jonas, Phys. Rev. A **62**, 033820 (2000).
[19] M. Zanni *et al.*, Proc. Natl. Acad. Sci. U.S.A. **98**, 11 265 (2001).
[20] J. D. Hybl, Y. Christophe, and D. M. Jonas, Chem. Phys. **266**, 295 (2001).